Structural analysis of the intermetallic surface compound $CePt_5$/Pt(111)

Jeannette Kemmer,[1,*] Christian Praetorius,[1,*] Andreas Krönlein,[1] Pin-Jui Hsu,[1] Kai Fauth,[1,2] and Matthias Bode[1,2]

[1]*Physikalisches Institut, Universität Würzburg, Am Hubland, 97074 Würzburg, Germany*

[2]*Wilhelm Conrad Röntgen-Center for Complex Material Systems (RCCM), Universität Würzburg, Am Hubland, D-97074 Würzburg, Germany*

(Received 25 July 2014; revised manuscript received 13 October 2014; published 3 November 2014)

We report on a detailed low-energy electron diffraction (LEED) and low-temperature scanning tunneling microscopy (STM) study of the intermetallic surface compound $CePt_5$ on Pt(111). Depending on the thickness we observe various diffraction patterns and superstructures. In the low-thickness regime a slightly compressed (2×2) superstructure is aligned along the $\langle 1\bar{1}0 \rangle$ direction of the Pt(111) substrate. STM reveals another, much larger superstructure with a periodicity of (9.02 ± 0.45) nm presumably responsible for the strongly broadened LEED spots. At about 3 unit cells (u.c.) the surface is dominated by a $(3\sqrt{3} \times 3\sqrt{3})R30^\circ$ pattern as revealed by LEED satellites and Fourier-transformed high-resolution STM images. It is interpreted as a moiré pattern between the film and the substrate. We precisely determine the superstructure of the intermetallic film to $(\frac{10}{9}\sqrt{3} \times \frac{10}{9}\sqrt{3})R30^\circ$ with respect to the Pt(111) substrate. Above 3 u.c. the satellites progressively disappear. A model is developed that consistently describes this thickness-dependent transition. For $CePt_5$ films with a thickness between 6 and 11 u.c. the lattice of the compressed (2×2) superstructure rotates back into the substrate's $\langle 1\bar{1}0 \rangle$ directions.

DOI: 10.1103/PhysRevB.90.195401 PACS number(s): 68.35.bd, 68.35.Ct, 68.37.Ef, 61.05.J−

I. INTRODUCTION

Although a topic of research for several decades already [1], the interaction of strongly localized f electrons with itinerant conduction bands remains a subject of considerable interest [2]. In particular, the formation of coherent heavy quasiparticle bands has recently been intensively investigated because of their important role in quantum criticality [3,4], spin-density wave instabilities [5], and the formation of coherent Kondo lattices [6,7]. In particular, ordered heavy-electron intermetallic compounds containing cerium, ytterbium, or other $4f$ elements have attracted considerable interest as some of them combine signatures of a local-moment state at high temperatures with the onset of coherent interaction with itinerant electrons at low temperatures [8].

Among these $4f$ intermetallic compounds, the Ce-Pt surface systems [9] have repeatedly been investigated regarding their electronic properties [7,10–13]. The phase diagram of bulk binary Ce-Pt alloys exhibits a number of stable intermetallic phases which display a variety of electronic and magnetic ground state properties. Stoichiometric CePt, for example, is a Kondo lattice material that orders ferromagnetically at low temperature and shows signs of quantum criticality at elevated pressure [14].

The crystallographic structure of the most Pt-rich bulk phase, $CePt_5$, consists of alternating layers of $CePt_2$ and a kagome lattice with three Pt atoms per unit cell. It orders antiferromagnetically at very low temperature and no signs of Kondo behavior were found in the paramagnetic regime [15]. Nevertheless, when grown as a surface intermetallic film on Pt(111) the formation of a coherent low-energy heavy-fermion band has recently been observed in $CePt_5$ films by means of high-resolution photoelectron spectroscopy near the Fermi level [7].

Previous structural investigations of the intermetallic phases that form upon deposition of metallic cerium onto Pt(111) and subsequent annealing revealed a rich variety of atomic surface structures, but also produced rather conflicting results [16–19]. An overview is summarized in Table I. For example, at low coverages up to an intermetallic film thickness of about 1 unit cell (u.c.) of $CePt_5$, Baddeley *et al.* [17] describe a $(5.6 \times 5.6)R30^\circ$ low-energy electron diffraction (LEED) pattern, the real-space periodicity of which they also observe by scanning tunneling microscopy (STM). In contrast, Tang *et al.* [16] and Essen *et al.* [19] report on the observation of the unchanged Pt(111) diffraction pattern for films of similar thickness.

Such conflicting reports can also be found for the coverage range between 1 and 2 u.c. of $CePt_5$. Here, Essen *et al.* report on the observation of what they call an "ideal (2×2) LEED pattern"[19], whereas according to Tang *et al.* [16] the diffraction pattern is contracted to (1.94×1.94) and Baddeley *et al.* find the superposition of a (2×2) structure and the above-mentioned $(5.6 \times 5.6)R30^\circ$ LEED pattern [17].

Somewhere between 3 and 5 u.c. of $CePt_5$ the appearance of LEED satellites was unanimously reported, indicating the formation of a superstructure [20] that is rotated by 30° with respect to the underlying Pt(111) substrate. However, the exact periodicity of this superstructure and the critical coverage required for its formation considerably vary across the literature [16–19]. For example, Essen *et al.* [19] mention a $(1.98 \times 1.98)R30^\circ$, and Baddeley *et al.* [17] a $(1.8 \times 1.8)R30^\circ$ which they discuss as a potential $(\sqrt{3} \times \sqrt{3})R30^\circ$ pattern. Furthermore, Tang *et al.* [16] report on the observation of a $(5.2 \times 5.2)R30^\circ$ satellite pattern, which they interpret as a consequence of the lattice mismatch between the substrate and the intermetallic film.

Finally, at much higher coverage of nominally 8 u.c. of $CePt_5$/Pt(111) a similar $(1.1\sqrt{3} \times 1.1\sqrt{3})R30^\circ$ pattern was observed by Garnier *et al.* [18]. We are not aware of any model that would consistently explain the observed superstructures. At even higher coverages typically starting at about 6 u.c. either a perfect [17] or compressed $(2 \times 2)R30^\circ$

*Corresponding authors (both authors contributed equally): jeannette.kemmer@physik.uni-wuerzburg.de; christian.praetorius@physik.uni-wuerzburg.de

TABLE I. The table summarizes the film-thickness-dependent LEED and STM results obtained in Refs. [16,17,19] together with the findings of the study presented here. Structures are labeled *A*–*E* following the nomenclature of Ref. [17].

Thickness range	Experimental technique	Tang *et al.* [16]	Baddely *et al.* [17]	Essen *et al.* [19]	This study
<2 u.c.	LEED	(1×1)	$(5.6 \times 5.6)R30^\circ$ and weak (2×2)	Ideal (2×2)	Faint (2×2)
	STM	—	Structure *A*	—	Nonperiodic (np)
2 u.c.	LEED	(1.94×1.94) with satellites	(2×2) and similar to $(5.6 \times 5.6)R30^\circ$	Ideal (2×2) and $(1.98 \times 1.98)R30^\circ$	(1.98×1.98)
	STM	—	Structures *A*/*B*/*C*	—	Structure *B*
3 u.c.	LEED	(1.96×1.96) with satellites	(2×2) and similar to $(5.6 \times 5.6)R30^\circ$	$(1.98 \times 1.98)R30^\circ$ and (2×2)	$(\frac{10}{9}\sqrt{3} \times \frac{10}{9}\sqrt{3})R30^\circ$ with satellites
	STM	—	Structures *A*/*B*/*C*	—	Structure *C*
4 u.c.	LEED	—	(2×2) with satellites	$(1.98 \times 1.98)R30^\circ$	Compressed $(2 \times 2)R30^\circ$
	STM	—	Structure *C*	—	Structure C'
5–10 u.c.	LEED	$(1.96 \times 1.96)R30^\circ$ and (1.96×1.96)	(2×2) and $(2 \times 2)R30^\circ$	(1.98×1.98) and $(1.98 \times 1.98)R30^\circ$	Compressed (2×2) and $(2 \times 2)R30^\circ$
	STM	—	Structures *D* and *E*	—	Structures *D* and C'
>10 u.c.	LEED	(1.96×1.96)	—	—	Compressed (2×2)

structure [16,19] has been observed, which eventually rotates back.

In this contribution we present a combined LEED and STM study of the surface structures that evolve when metallic Ce is deposited on Pt(111) and subsequently annealed for surface alloying. The use of reciprocal and real-space techniques results in a comprehensive understanding of the surface structures of thin $CePt_5$ on Pt(111). In order to allow for a reliable comparison with earlier results [16–19], the details of our experimental parameters including LEED and STM setups, sample preparation and Ce deposition procedures, and the film thickness calibration will be described in Sec. II. After a short introduction to the clean Pt(111) substrate (Sec. III A) we will present and discuss data obtained on films in the low- (Sec. III B), intermediate- (Sec. III C), and high-thickness regimes (Sec. III D), being specified as $CePt_5$ films of 1–2 u.c., 3–5 u.c., and 6–15 u.c., respectively. On the basis of a detailed comparison of LEED data with STM images analyzed in real and reciprocal space we have investigated the evolution of strain, strain relief, and lattice parameters over a significant range of surface intermetallic thickness. From the analysis of both the $CePt_5$ lattice and the characteristics of superstructures (moiré patterns) we are able to provide a structural model which allows for a consistent picture of $CePt_5$ thin film formation on Pt(111).

II. EXPERIMENTAL SETUP AND PROCEDURES

A. LEED

The LEED experiments were performed in two different ultrahigh vacuum (UHV) chambers with base pressures of $p \approx 5 \times 10^{-10}$ mbar. Both LEED devices were standard four-grid instruments equipped with LaB_6 cathodes. The fluorescent screens had an outer radius of 68 mm and an opening angle of $2\theta = 100^\circ$. The coherence length of such instruments typically amounts to $l_c \approx 10$ nm [21]. All LEED data were recorded at room temperature. The diffraction pattern was independent of the lateral positioning of the sample relative to the LEED optics, thereby confirming sample homogeneity. Images were taken with a commercial digital camera. The settings of the LEED optics were optimized for the clean substrate and then kept constant for the following experiments on alloyed samples. The same was done for the azimuthal specimen orientation, thereby assuring comparability of LEED patterns taken on different samples.

The LEED pattern is a projection of the reciprocal surface lattice of the sample and can be used to determine lattice constants. However, imperfect rotational and translational alignment introduces distortions to the pattern. Furthermore, the photographic imaging of the curved fluorescent screen is an imperfect projection of the pattern, if the distance between screen and camera is not very large as compared to the screen radius [22]. Given the geometry and the uncertainties of our experimental LEED setup, we estimate the error in the determination of the absolute lattice constant to 5%–7%.

This uncertainty is of the same order of magnitude as the film-thickness-dependent lattice constant changes expected for the surface intermetallic $CePt_5$ on Pt(111) we are looking for in the present work. Therefore, any determination of absolute lattice constants would be highly problematic. Similar limitations may be responsible for the considerable spread of lattice constants reported in literature [16–19]. In order to increase the significance of experimental results, in the present work we will compare relative length scales obtained from single LEED images.

The Pt(111) substrate (MaTeck GmbH) was cleaned by numerous cycles of Ar^+ ion sputtering at a beam energy of $E = 1$ keV and subsequent annealing to $T = 1170$ K. Oxygen roasting was omitted in order to avoid any unwanted oxidation of the Ce evaporant which was installed in the same chamber. The cleanliness of the substrate was confirmed by the

absence of C and O signatures in Auger electron spectroscopy. Cerium (purity 99.5%, MaTeck GmbH) was evaporated from a thoroughly degassed tungsten crucible with a commercial electron beam evaporator. After Ce deposition onto the substrate at room temperature the film was subsequently annealed to $T \approx 970$ K for 10 min. This well-established preparation procedure is known to result in highly ordered surface intermetallics [7,16–19].

B. STM

STM experiments were performed in a UHV chamber with a base pressure of $p \leqslant 5 \times 10^{-11}$ mbar. The clean Pt(111) surface was prepared by cycles of Ar^+ ion sputtering at an ion energy of 500 eV and annealing up to 1300 K for several minutes. Since—in contrast to LEED experiments—the Ce evaporator can be retracted and sealed off from the preparation chamber, occasional annealing in an oxygen atmosphere ($p_{O_2} \leqslant 1 \times 10^{-7}$ mbar) at 1100 K was performed. The cleanliness of the substrate was confirmed by STM. For Ce evaporation we used a tungsten crucible with a commercial e-beam evaporator cooled with liquid nitrogen. During evaporation at $p < 5 \times 10^{-10}$ mbar the substrate remained at room temperature. Subsequently annealing up to 1000 K produces the surface intermetallic compound $CePt_5$/Pt(111) [17]. After preparation, the sample was immediately transferred into a home-built low-temperature scanning tunneling microscope (LT-STM) (operation temperature $T = 5.5$ K). In order to exclude that temperature-dependent phase transitions influence the film structure, we also performed measurements on films at room temperature. Indeed, results were basically identical to comparable measurements on films which were cooled down to 5 K. For topographic images, the LT-STM was operated in the constant-current mode with the bias voltage (U) applied to the sample. Differential conductance maps were acquired by lock-in technique with a small voltage modulation U_{mod} added to the tunneling voltage (frequency $f = 5.777$ kHz).

C. Thickness calibration

The main topic of this contribution is surface structures of $CePt_5$/Pt(111) which can be controlled by the amount of Ce that is deposited prior to alloying. In LEED experiments the evaporation rate was measured immediately prior to the deposition by means of a quartz microbalance that was moved into the sample position. By recording the frequency change versus deposition time the mass of the deposited Ce per area can be determined [23]. This allows for an accurate calculation to the Ce atoms flux per Pt(111) surface unit cell. We estimate the error of this procedure to about ±5%.

Often in thin film growth the amount of deposited material is specified in units of monolayers [16,17,19]. Instead, in the present work we have chosen a different unit for the film thickness t, i.e., the number of $CePt_5$ u.c. Note, that the number of unit cells given throughout this paper refers to the average thickness rather than to the local thickness. In our opinion this unit is more meaningful since we are dealing with intermetallic alloy films where the number of three-dimensional $CePt_5$ unit cells, which contain a single Ce atom, describes the sample in its final state. The two units—monolayers and unit cells—can be easily converted into each other by considering the $CePt_5$ surface unit cell area, which is almost precisely four times as large as for the Pt(111) surface, and the fact that the nearest-neighbor distance of Ce/Pt(111) is 1.4 times larger than that of the substrate [17]. Hence, one monolayer of Ce deposited onto the substrate corresponds to approximately two Ce atoms per four Pt(111) surface unit cells, which would lead to a film thickness of $t = 2$ u.c. A comparison of our LEED data to the literature confirms the consistency of this approximate conversion.

In contrast, the Ce deposition rate in STM experiments was calibrated by deposition onto W(110). Similar to experiments on Gd and Tb on W(110) we observed monatomic chains. They consist of rare-earth-metal elements that form $(n \times 2)$ superstructures where n decreases with increasing coverage [24,25]. The deposition rate was calculated based on an assessment of the chain length and density. This procedure is much less accurate and yields a nominal deposition rate equivalent to 1 u.c. of $CePt_5$/Pt(111) per minute. Good agreement between LEED and STM results is obtained under the assumption that the nominal deposition rate in STM experiments is underestimated by about 25%. Therefore, for the data presented below, we assume that 40 s of Ce deposition corresponds to the formation of 1 u.c. of $CePt_5$ after annealing.

III. RESULTS AND DISCUSSION

A. Pristine Pt(111) substrate

As shown in Fig. 1(a) the preparation procedures described above result in a Pt(111) substrate that is characterized by a sharp LEED pattern with bright diffraction spots and a low background intensity. The threefold rotational symmetry of Pt(111) becomes apparent under variation of the electron beam energy (not shown here). The azimuthal orientation and the resulting planar crystallographic directions of the substrate are shown in Fig. 1 for reference.

A typical large-scale STM image displaying three atomically flat terraces is shown in Fig. 1(b). The terraces are separated by monatomic step edges with a height $h = (0.215 \pm 0.012)$ nm, consistent with literature [26]. White arrows mark the low-index crystallographic directions within the Pt(111) surface. The length of these arrows is proportional to the respective nearest-neighbor and next-nearest-neighbor atomic distances. The atomic resolution STM image of Fig. 1(c) was obtained on a defect-free surface region and displays the hexagonal symmetry of the Pt(111) surface layer in real space. The inset shows the Fourier transformation (FT) of the real-space image. It confirms the hexagonal structure of the surface with three equivalent $\langle 1\bar{1}0 \rangle$ directions. The nominal nearest-neighbor distance of 0.277 nm [26] was used for calibrating the lateral sensitivity of our LT-STM. The error between different experimental runs is estimated to approximately 5%, mainly caused by piezocreep and thermal drift.

B. Low-thickness regime ($t \approx 1$–2 u.c.)

The preparation of samples with a nominal thickness of $t \approx 1$ u.c. leads to the appearance of faint superstructure spots superimposed onto the diffraction pattern of the substrate

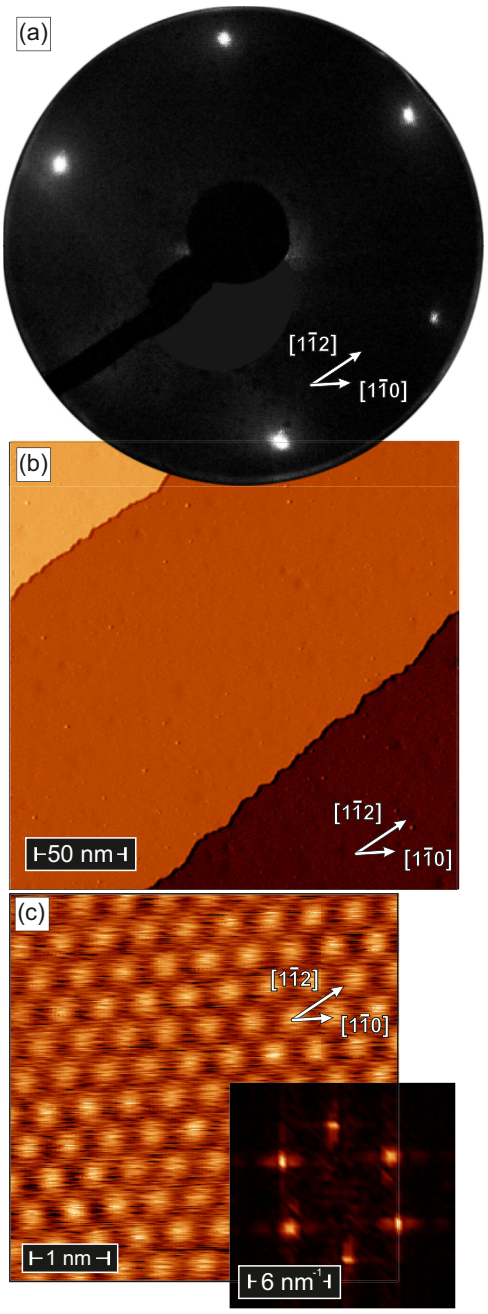

FIG. 1. (Color online) Pristine Pt(111). Arrows mark the crystallographic directions. (a) LEED image obtained at a primary electron energy $E_p = 63$ eV. The missing spot in the lower left is covered by the electron gun. (b) STM topography showing three atomically flat terraces separated by two monoatomic step edges (scan parameters: $U = +1.0$ V, $I = 300$ pA). (c) Atomic resolution image as obtained on a defect-free surface area ($U = +1.0$ mV, $I = 90$ nA). The corresponding FT is shown in the inset.

(not shown here). Within error the lattice constant of the superstructure amounts to twice that of Pt(111). The main sources of uncertainties in this assignment are the considerable broadness and the relatively low intensity of the superstructure spots. In contrast to the Pt(111) substrate the superstructure shows sixfold rotational symmetry under variation of the beam energy. The same is true for all superstructures that are described below.

Upon increasing the film thickness to about $t \approx 2$ u.c. the superstructure pattern becomes more intense. Such a pattern is shown in Fig. 2(a). The diffraction spots are relatively broad and overlap the substrate spots. Nevertheless, the diffraction spots of the substrate can still be identified at electron energies where their threefold symmetry is apparent (not shown here). Direct comparison of the spot positions of the substrate and the film reveals that—in agreement with the data of Ref. [16] but in contrast to the results presented in Ref. [19]—the film lattice constant is slightly reduced with respect to a perfect (2×2) superstructure. Since quantification is complicated by the overlap of the spots of film and substrate, an alternative route for the determination of the lattice constant was chosen. It will be described in detail in Sec. III C.

A topographic STM image (scan range: 300 nm $\times$ 300 nm) of a $CePt_5$ intermetallic film with average thickness of 2 u.c. is shown in Fig. 2(b). We observe four different surface structures. In accordance with Ref. [17] the two structures with the largest relative weight were labeled *B* and *C*. A differential conductance map of structure *B* at higher magnification and the corresponding FT are shown in Figs. 2(c) and 2(d), respectively. (Unit cell resolution can also be seen in the topography, but the contrast is significantly improved in the differential conductance map.) Besides a hexagonal structure with a periodicity of (0.562 ± 0.028) nm [green symbols in Figs. 2(c) and 2(d)] with nearest-neighbor maxima arranged along the $\langle 1\bar{1}0 \rangle$ direction of the Pt(111) substrate, another superstructure with a much larger periodicity of (9.02 ± 0.45) nm can be recognized. Note that this superstructure, which is marked by blue symbols in Figs. 2(c) and 2(d), exhibits the same orientation as the bare Pt(111) substrate.

The superstructures observed by LEED [Fig. 2(a)] and by STM [Figs. 2(b)–2(d)] are well in line regarding the (2×2) atomic structure of the terminating surface. This (2×2) superstructure is consistent with a kagome lattice of the terminating Pt layer. In addition, STM observes a large-scale superstructure which is not discernible in LEED data. There are two factors which prevent identification of those structures in LEED: First, due to the large periodicity in real space the spacing of the superstructure diffraction spots in *k* space would be very narrow, as can be seen in the FT-STM image of Fig. 2(d). Probably, the superstructure spots cannot be resolved by our LEED instrument but lead to the significant broadening of the main spots observed in Fig. 2(a). Second, the periodicity of the superstructure pattern of (9.02 ± 0.45) nm is of the order of the coherence length l_c of the LEED instrument [21]. Therefore, a periodicity that large might lead to a very weak coherent diffraction pattern with substantial peak broadening.

We identify structure *B* of Fig. 2 as the same structure already analyzed by Baddeley *et al.* [17] which was interpreted as a several-layer-thick, $CePt_2$-terminated, and not fully relaxed intermetallic compound. In contrast to this earlier report, we observe this structure only for short deposition times corresponding to $t < 2.5$ u.c. Furthermore, we find a long-range periodicity which is slightly smaller than the $\approx$10 nm reported by Baddeley *et al.* [17]. The second periodic structure, named *C*, was also observed by Baddeley *et al.* [17]. It will be discussed in Sec. III C in detail. The reconstruction

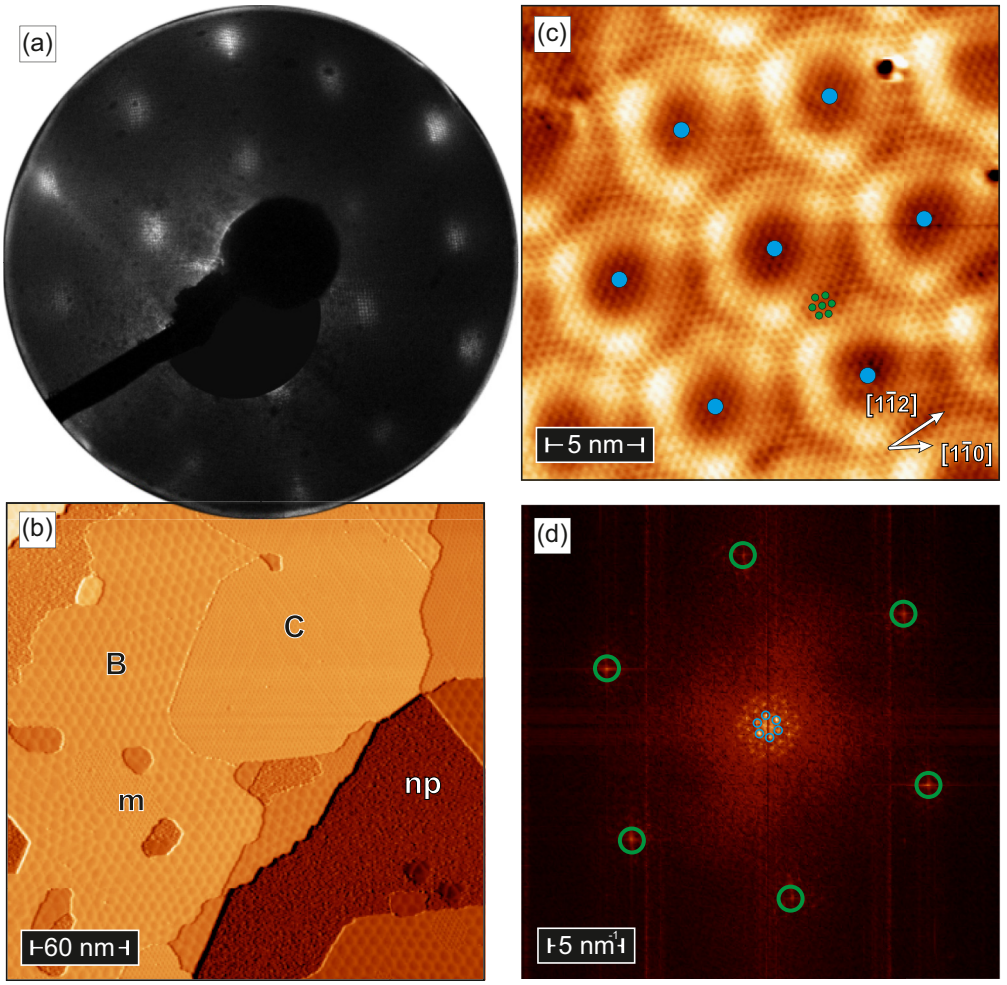

FIG. 2. (Color online) 2 u.c. $CePt_5$ on Pt(111). (a) LEED pattern ($E_p = 63$ eV) and (b) large-scale STM topography showing structures B, C, the nonperiodic (np) structure, and a minority surface reconstruction m (scan parameters: $U = +1.0$ V, $I = 300$ pA). (c) High-resolution differential conductance map and (d) the FT of structure B. The superstructure pattern and the lattice of $CePt_5$/Pt(111) are marked in blue and green, respectively.

labeled m is a minority phase that covers only a few percent of the surface. It will not be discussed in the following because of its negligible contribution to the overall film morphology. Finally, a nonperiodic (np) reconstruction is also observed.

C. Intermediate-thickness regime ($t \approx 3$–5 u.c.)

At a thickness of $t \approx 3$ u.c. distinct changes as compared to the low-thickness regime are observed in the LEED pattern, as shown in Fig. 3(a). While the superstructure lattice constant remains approximately twice the Pt(111) surface lattice constant, the pattern appears rotated by $\varphi = 30^\circ$, thereby forming a compressed $(2 \times 2)R30^\circ$ atomic lattice of the intermetallic surface compound with respect to the Pt(111) substrate. In other words, unit cells of the (2×2) structure are now aligned along the $\langle 1\bar{1}2 \rangle$ directions of the substrate. Details of this compression will be discussed below. Furthermore, the diffraction spots become much sharper and are accompanied by satellite spots. The distance between main and satellite spots is evaluated to 0.187 times the distance between the main spots, which equals $1/(3\sqrt{3})$ within 3%. The satellite pattern can thus be interpreted as resulting from a $(3\sqrt{3} \times 3\sqrt{3})R30^\circ$ superstructure of the intermetallic surface compound.

As shown in the large-scale STM image of Fig. 3(b) the surface of an intermetallic film with a thickness of 3 u.c. is strongly dominated by structure C. Only tiny fractions of the surface area exhibit either structure B or the np structure (black area). These are visible in the two holes in the top and middle of Fig. 3(b), respectively. The inset presents an atomically flat area at higher magnification. We can recognize several bright lines which are oriented along $\langle 1\bar{1}0 \rangle$ directions as highlighted by dashed lines and surround ordered surface areas with typical lateral dimensions of 10 . . . 20 nm.

Figure 3(c) shows a high-resolution STM image of structure C. The blue spots in Fig. 3(c) mark a large-scale superstructure which exhibits a periodicity of (2.87 ± 0.14) nm and is aligned along the $\langle 1\bar{1}0 \rangle$ directions. Green spots represent the compressed $(2 \times 2)R30^\circ$ surface structure of the terminating layer. Its nearest-neighbor distance is determined to (0.548 ± 0.027) nm which agrees well with the kagome lattice of $CePt_5$. Note that this atomic scale lattice is rotated by 30° with respect to both the bare Pt(111) surface and the large-scale superstructure

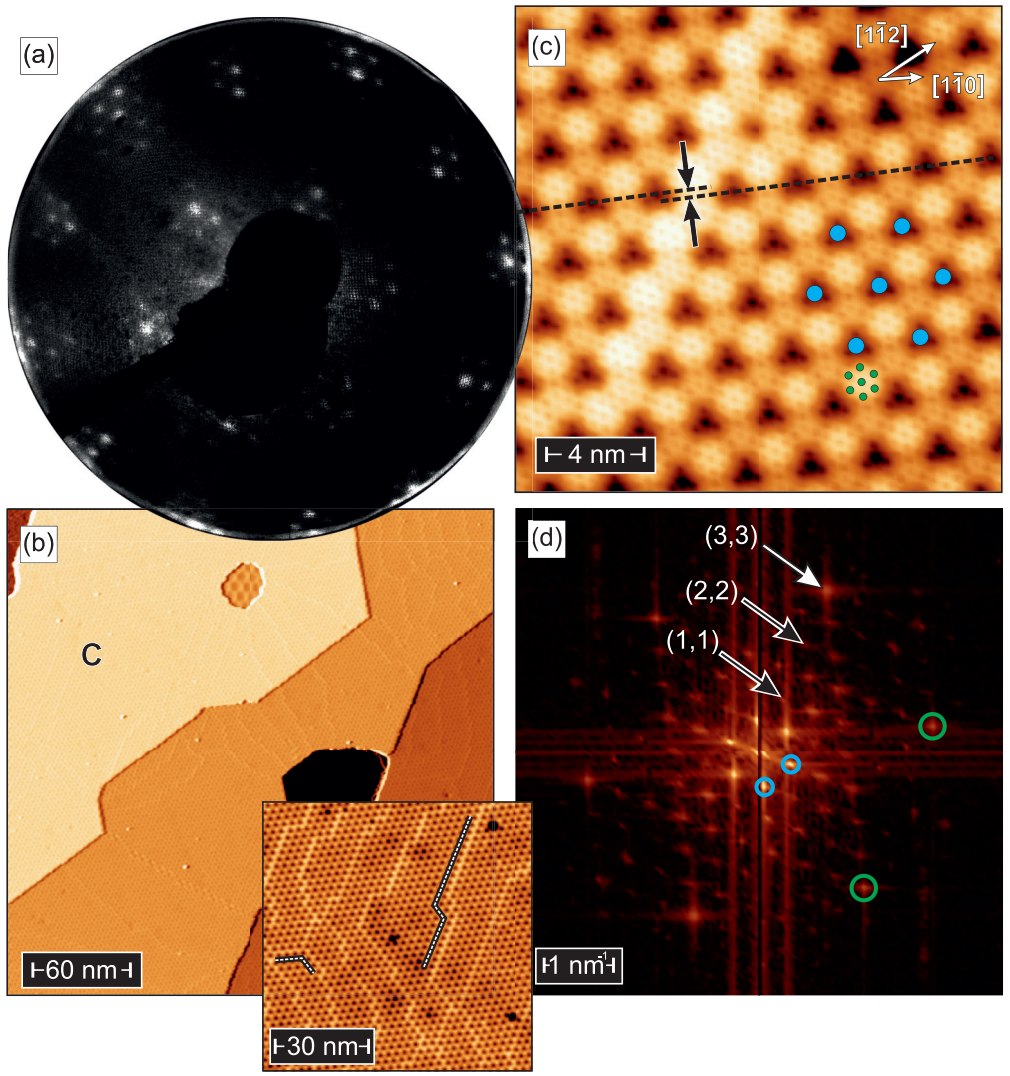

FIG. 3. (Color online) 3 u.c. $CePt_5$ on Pt(111). (a) LEED image ($E_p = 63$ eV) and (b) STM image of a surface dominated by structure C. Minor surface areas display structure B and the np structure (black). The inset shows the surface of an atomically flat terrace with domain walls (some of which are highlighted by white lines) oriented along the $\langle 1\bar{1}0\rangle$ directions of the Pt(111) substrate (scan parameters: $U = +1.0$ V, $I = 300$ pA). (c) High-resolution image and (d) its FT with blue and green marks illustrating the superstructure and the atomic lattice of $CePt_5$/Pt(111), respectively. Note that the atomic lattice is rotated by 30° relative to Pt(111). The moiré pattern forms a $(3\sqrt{3} \times 3\sqrt{3})R30°$ superstructure of the atomic lattice as highlighted by the (1,1) and (2,2) spots (marked by black arrows). The (3,3) spot (white arrow) coincides with the (1,0) spot of the intermetallic film.

of structure C, consistent with the LEED pattern of Fig. 3(a). These results are in excellent agreement with Baddeley *et al.* [17] who found an interatomic spacing of (0.512 ± 0.015) nm for structure C and a superstructure rotated by 30° and with a periodicity of (2.68 ± 0.08) nm.

In Fig. 3(c) one of the previously mentioned bright lines crosses the image from the lower left corner towards the upper right. As indicated by the dashed lines which connect minima of the superstructure, the lattices in the left and the right parts of the image are slightly shifted relative to each other. From this high-resolution image we can conclude that the bright lines represent domain walls separating superstructures which are shifted with respect to one another. In the case present in Fig. 3(c) this shift amounts to one lattice constant of the $(2 \times 2)R30°$-reconstructed $CePt_5$/Pt(111) surface compound.

In the FT of Fig. 3(c), which is shown in Fig. 3(d), the green (blue) dashed circles mark the $(2 \times 2)R30°$-reconstructed atomic lattice (superstructure spots). Around the atomic lattice spots the superstructure spots can be verified. Black arrows in the FT are pointing to the (1,1) and (2,2) spots of the superstructure. Apparently, the (3,3) spot (white arrow) of this superstructure coincides with the (1,0) spot of the intermetallic film which allows the unambiguous identification of the superstructure as $(3\sqrt{3} \times 3\sqrt{3})R30°$. Overall, the FT-STM image of Fig. 3(c) is in excellent correspondence with the LEED pattern of Fig. 3(a).

A similar $R30°$ structure was also observed for the $CeAu_2$ monolayer on Au(111) and interpreted as a moiré pattern [27]. In contrast, the LEED satellite pattern of Fig. 3(a) was interpreted as resulting from multiple scattering at two lattices by Essen *et al.* [19], i.e., a (2×2) and a $(1.98 \times 1.98)R30°$

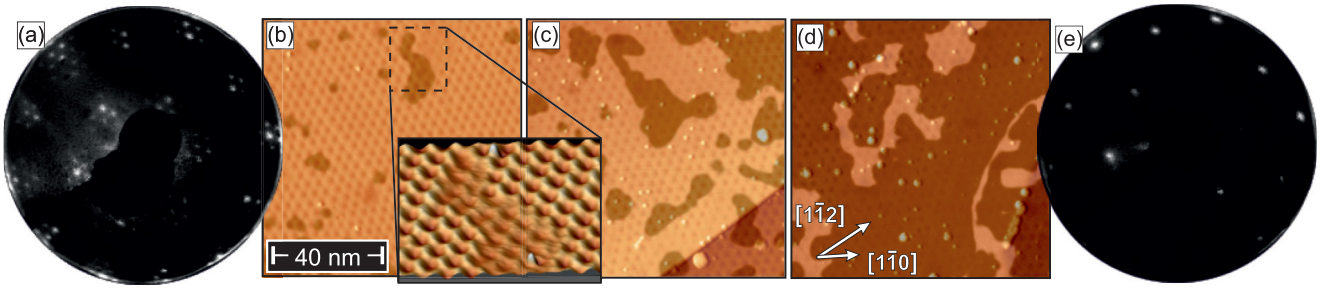

FIG. 4. (Color online) (a) LEED image ($E_p = 63$ eV) and (b) STM topography of a 3 u.c $CePt_5$ intermetallic film on Pt(111). The surface is almost completely covered with structure C which is highlighted by a bright tone in (b). The inset shows a rendered three-dimensional representation of the surface area within the box. (c) At 3.75 u.c. $CePt_5$ the surface fraction covered by structure C has decreased significantly. This is compensated by a larger fraction of the surface being covered by structure C' (dark tone). (d) and (e) show an STM image and the LEED pattern of 4.5 u.c. $CePt_5$/Pt(111) which are dominated by structure C'.

superstructure with respect to the Pt substrate. These lattices may coexist laterally, as proposed in Ref. [19], or vertically. In our opinion a coexistence is not consistent with the data presented here (and in Ref. [19]) since the first-order spots of the (2×2) pattern, which were clearly visible at lower film thickness in Fig. 2(a), are missing in Fig. 3(a). Furthermore, such a multiple scattering diffraction pattern requires the two lattices to laterally coexist on the length scale of the LEED coherence length l_c. Our STM results indicate that the domain size exceeds 10 nm [cf. inset of Fig. 3(b)].

Alternatively, the results may be explained by two lattices that coexist on top of each other. At this point it shall be mentioned, however, that the geometrical construction of the diffraction spots for the multiple scattering mechanism is the same as for moiré pattern formation. Hence, based on LEED data alone the two indistinguishable scenarios are as follows: (i) multiple scattering of electrons at the interface between a substrate and a flat film with slightly different lattice constants and (ii) the formation of a moiré pattern due to a periodic modulation of the atomic adsorption sites of the film material, the lattice constant of which is slightly misfit with respect to the substrate material. They can be distinguished based on the different surface morphologies expected in STM experiments. While a flat surface is expected for (i), moiré pattern formation [scenario (ii)] is expected to result in a significant buckling of the surface. Indeed, our STM results clearly show a surface height modulation of the order of 50–100 pm. It is therefore most likely that the satellite spots in LEED arise from diffraction at the moiré lattice.

The consistent interpretation of the satellite spots in LEED and the moiré pattern in STM as arising from a combination of substrate and the rotated film lattice allows one to derive the precise relation between the three lattices. As argued above, the film lattice is rotated by 30° with respect to both the substrate and the moiré lattices. The relation between the film and moiré lattice constants was evaluated to $a_{\text{moiré}} = 3\sqrt{3}a_{\text{film}}$. Furthermore, the mechanism that produces a moiré pattern requires that the moiré lattice constant is an integer multiple of the substrate lattice constant, $a_{\text{moiré}} = na_{\text{sub}}$. Hence, $a_{\text{film}} = n\sqrt{3}/9a_{\text{sub}}$. Since both our LEED and STM data indicate that $\sqrt{3}a_{\text{sub}} < a_{\text{film}} < 2a_{\text{sub}}$, it follows that $n = 10$. Thus, the moiré pattern is a (10×10) superstructure of the substrate lattice, while the film lattice can be traced back to a $(\frac{10}{9}\sqrt{3} \times \frac{10}{9}\sqrt{3})R30°$ reconstruction with respect to the substrate. The assignment of a similar LEED pattern as an approximate $(1.1\sqrt{3} \times 1.1\sqrt{3})R30°$ superstructure that was reported by Garnier *et al.* [18] is in close agreement to this result. Under the assumption that the lattice constant of the substrate that contributes to the moiré pattern is not influenced by the presence of the film and equals the bulk value, the lattice constant of the intermetallic film at $t \approx 3$ u.c. can thus be evaluated to $a_{\text{film}} = 0.534$ nm. This corresponds to a compression of the $CePt_5$ bulk value by 0.5%.

As already reported by Essen *et al.* [19], the LEED patterns of intermetallic films in the thickness range $t \approx 2 \ldots 4$ u.c. occasionally showed coexistence of the patterns presented in Figs. 2(a) and 3(a). In analogy to their study, we have performed a relative lattice constant determination of the two patterns from individual LEED images. The lattice constants are different by a factor of 0.97 ± 0.03, with the smaller lattice constant associated with the thicker film. Based on the determination described above, this allows the conclusion that the lattice constant at $t \approx 2$ u.c. amounts to 0.551 nm, which corresponds to a (1.98×1.98) superstructure.

Figure 4 shows the evolution of LEED and STM data as the $CePt_5$ intermetallic film thickness is increased from 3 u.c. to 4.5 u.c. The sequence starts with the LEED pattern of structure C at 3 u.c. which is rotated and displays satellite spots characteristic for the $(3\sqrt{3} \times 3\sqrt{3})R30°$ superstructure [Fig. 4(a)]. Correspondingly, the STM image of an equivalent sample presented in Fig. 4(b) is rather homogeneously covered with the associated moiré pattern which has a periodicity of (2.87 ± 0.14) nm and a corrugation of about 80 pm. Only a small surface fraction is covered by another structure C' [highlighted by a dark tone in Fig. 4(b)] which exhibits the same periodicity and orientation as structure C but a lower corrugation of around 40 pm only. The inset of Fig. 4(b) shows a rendered three-dimensional representation of a C' patch which is surrounded by structure C at higher magnification. Detailed analysis reveals that the moiré patterns of the two structures are shifted by 1/3 of the moiré periodicity along the $\langle 1\bar{1}0 \rangle$ directions. As can be seen in the thickness-dependent series of typical surface morphologies of $CePt_5$ intermetallic films on Pt(111) displayed in Figs. 4(b)–4(d) the surface fraction of structure C' increases at the expense of C, while C' covers only about 5% . . . 10% at a film thickness of 3 u.c.

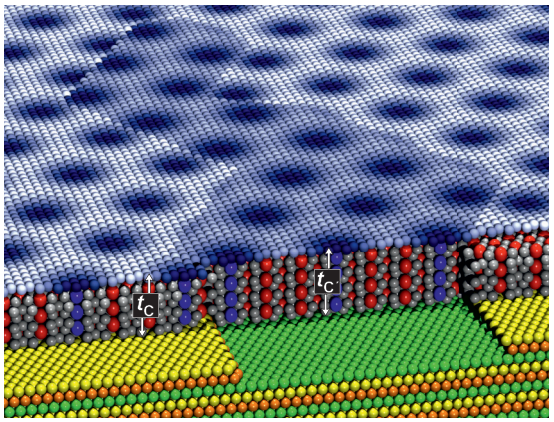

FIG. 5. (Color online) Structural model of structures C and C' observed for $CePt_5$/Pt(111). In correspondence with the STM images presented in Figs. 4(b) and 4(c) bright (dark) surface areas illustrate structure C (C'). White, yellow, brown, and green spheres represent the Pt atoms and the red (between Pt atoms) and blue (top of Pt atom) the Ce atoms.

[Fig. 4(b)], its fraction increases to 30% . . . 40% at 3.75 u.c. [Fig. 4(c)], and reaches more than 80% at 4.5 u.c. [Fig. 4(d)]. This thickness-dependent transition from structure C to C' is accompanied by LEED satellite spots which get progressively weaker and eventually vanish above $t \approx 4$ u.c. [Fig. 4(e)]. This is consistent with our calculation performed within the kinematic approximation which indicates that the satellite intensity scales with the square of the corrugation amplitude.

Figure 5 presents a model which can explain the different corrugations found on structures C and C' as well as the phase shift of their respective moiré patterns. It shows a cross-sectional view of approximately the sample area shown in the rendered perspective representation presented in the inset of Fig. 4(b). Green, yellow, and brown spheres illustrate A, B, and C layers of *fcc*-stacked Pt(111) substrate, respectively. The central region of the substrate exhibits two double-atomic step edges thereby exposing different (yellow and green) Pt atomic planes to the interface. This substrate is covered by a $CePt_5$ film which is visualized by gray and red/blue spheres representing Pt and Ce atoms, respectively. At this point it is important to recall that the formation of the moiré pattern is caused by the fact that the lattice constants of the $CePt_5$ intermetallic film and the Pt(111) substrate slightly differ. Therefore, depending on their lateral position Ce atoms will occupy different sites. In our model of Fig. 5 blue spheres represent Ce atoms that are placed on top of a Pt atom, while those located at threefold hollow sites between Pt atoms are shown as red spheres. In the given case the size and orientation of the moiré pattern amounts to $(3\sqrt{3} \times 3\sqrt{3})R30^\circ$, resulting in the alternation of two hollow (red) with one on-top site (blue) along the $\langle 1\bar{1}2 \rangle$ directions of the substrate.

The resulting surface corrugation is displayed in a white-blue color code. Our model which assumes that the thickness of the intermetallic compound differs by one unit cell, i.e., $t_C = n$ u.c. and $t_{C'} = (n+1)$ u.c., nicely reproduces two experimental observations made in Fig. 4. First, it is consistent with the finding that the moiré patterns of the two structures are shifted by 1/3 of their periodicity along $\langle 1\bar{1}0 \rangle$ directions. Second, it is well known that the corrugation of moiré patterns decreases with increasing film thickness [28,29], probably due to the partial relief of strain. We speculate that the same mechanism is at work here. It results in a reduction of the surface corrugation visible by STM and—as the intensity of the respective spots drops below our detection limit—the disappearance of the satellite pattern in LEED.

D. High-thickness regime ($t \approx$ 6–15 u.c.)

Interestingly, we find that the superstructure, the rotation of which we observed between 2 and 3 u.c., rotates back into the original direction of the Pt(111) substrate starting at a film thickness $t \gtrsim 6$ u.c. This back-rotation can clearly be recognized in the LEED patterns of Fig. 6 taken on films with a thickness (a) $t = 7$ u.c., (b) 8 u.c., and (c) 10 u.c. In addition to the rotated superstructure, a back-rotated pattern appears above a film thickness of $t \approx 6$ u.c. (not shown here). The lattice constants of the two coexisting patterns are the same within the given accuracy. As visible in Figs. 6(a)–6(c) the relative intensity of the back-rotated pattern with respect to the rotated one increases with increasing thickness. At $t \approx 8$ u.c., the two patterns appear with equal intensities. Above $t \approx 11$ u.c. the rotated pattern is not visible anymore, leading to a pure nonrotated LEED image (not shown here). While Tang *et al.* [16] mention that the relative intensities "depend somewhat on the initial (Ce) coverage," here we report the monotonous transition from the rotated structure C' to a back-rotated superstructure, which is clearly visible in our LEED data.

This back-rotation can also be seen by STM. Figures 6(d) and 6(e) show the simultaneously recorded topographic STM image and a differential conductance map, respectively, of a 10 u.c. $CePt_5$ film. Figure 6(d) illustrates the surface reconstructions C' and a reconstruction named D previously reported by Baddeley *et al.* [17]. Those structural domains are separated from each other by domain boundaries which are decorated by protruding dots, possibly representing excess atoms. While the surface of structure C' appears rather flat in the topographic STM image of Fig. 6(d), the simultaneously taken differential conductance map [Fig. 6(e)] reveals that the characteristic moiré pattern of structure C' is still present. Structure D exhibits a bumpy surface with a corrugation of about 100 pm but no obvious periodicity. The black arrow in Fig. 6(d) marks a minority surface reconstruction, which covers only some percent of the surface and will therefore not be discussed here. The white arrow points to a dislocation line in structure D.

In the high-resolution image of structure C' [left panel of Fig. 6(f)] the moiré pattern is marked by blue dots and the $CePt_5$ unit cell by green dots. As can be seen by inspection of the corresponding FT (right panel), the unit cell and the moiré pattern are still rotated by 30° with respect to each other. The periodicities of the $CePt_5$ lattice and the moiré pattern are determined to (0.566 ± 0.028) nm and (2.87 ± 0.14) nm, respectively, in good agreement with structure C.

Figure 6(g) shows a high-resolution STM image (left panel) and its FT (right) of structure D. Again green symbols illustrate the unit cell in real and reciprocal space. For this structure no moiré pattern is observed. Our LEED and STM data show that for thick films the surface atomic lattice rotates back by 30°, i.e., nearest-neighbor atoms of the terminating

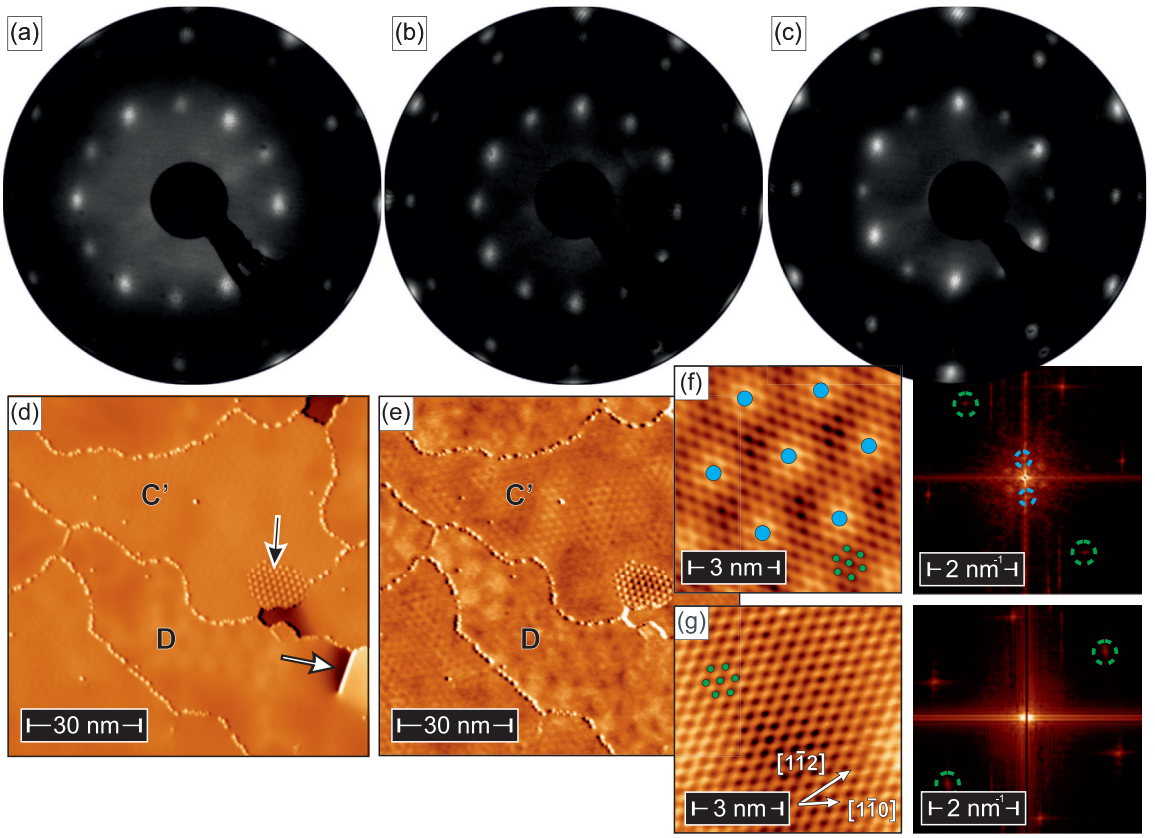

FIG. 6. (Color online) LEED patterns of $CePt_5$ films grown on Pt(111) with thickness (a) $t = 7$ u.c., (b) 8 u.c., and (c) 10 u.c ($E_p = 50$ eV). Note the rotation by 30°. (d) and (e) show the simultaneously recorded topographic STM image and differential conductance map, respectively, of a 10 u.c. $CePt_5$ film (scan parameters: $U = +1.0$ V, $I = 300$ pA, $U_{mod} = 10$ mV). Structures C' and D are separated by domain boundaries. The black arrow marks a minority structure of the surface and the white arrow points to a dislocation line. (f) and (g) High-resolution (left panel) and corresponding FT images (right) acquired on structures C' and D, respectively ($U = +1.0$ V, $I = 300$ pA). In either case blue and green marks indicate the moiré pattern and the $CePt_5$ unit cell, respectively.

atomic lattice of the $CePt_5$/Pt(111) are aligned along the $\langle 1\bar{1}0\rangle$ directions of the bare Pt(111) surface. The lattice constant is determined to (0.558 ± 0.028) nm, close to the bulk value reported for $CePt_5$ [9].

Several scenarios are conceivable for the interpretation of the LEED pattern and the STM images in this thickness regime. One possibility would be that—similar to the model presented in Fig. 5—the two phases, C' and D, are characterized by their different local thicknesses. In this case with increasing coverage we would expect a gradual change of their relative surface fraction from C' dominated at low coverage towards D dominated at very high coverage, in analogy to our findings in the intermediate thickness regime (cf. Sec. III C). Alternatively, the coexistence may also be explained by the two structures having very similar formation energies. Distinguishing between these two scenarios would require accessing the interface of the sample. While this is possible in principle by techniques such as x-ray scattering, the probing depths of LEED and STM are not sufficient in the high-thickness range, and the topic remains to be investigated in future studies.

IV. SUMMARY

In conclusion we have performed a combined LEED and STM investigation of the $CePt_5$ intermetallic alloy on Pt(111). For the low-thickness range up to about 2 u.c. the LEED pattern shows a slightly compressed (2×2) superstructure which exhibits sixfold symmetry and is strongly broadened as compared to the clean Pt(111) substrate. In addition to this approximate (2×2) superstructure, which is consistent with the kagome lattice of a Pt layer terminating the $CePt_5$ film, STM reveals another, much larger superstructure with a periodicity of (9.02 ± 0.45) nm presumably being responsible for the strongly broadened LEED spots. Both superstructures in combination constitute structure B. At about 3 u.c. the surface is dominated by the $(3\sqrt{3} \times 3\sqrt{3})R30°$ superstructure (C) as revealed by LEED satellites and Fourier-transformed high-resolution STM images. Structure C consists of a rotated superstructure and a moiré pattern with a periodicity of (2.87 ± 0.14) nm. It exhibits domains with a typical lateral size of 10 . . . 20 nm. We have precisely determined the superstructure of the intermetallic film to $(\frac{10}{9}\sqrt{3} \times \frac{10}{9}\sqrt{3})R30°$ with respect to the Pt(111) substrate. When increasing the $CePt_5$ coverage above 3 u.c. structure C transforms into structure C' and the satellites vanish, which is in line with the lower corrugation observed by STM. We present a model that consistently describes the transition from structure C to C' with increasing film thickness. For $CePt_5$ films with a thickness between 6 and 11 u.c. the lattice of the compressed (2×2) superstructure

rotates back into the substrate's orientation, leading to structure *D* the lattice constant of which closely matches bulk $CePt_5$.

ACKNOWLEDGMENT

This work has been funded by Deutsche Forschungsgemeinschaft within FOR 1162 (projects P5 and P7).

[1] G. R. Stewart, Rev. Mod. Phys. **56**, 755 (1984).
[2] H. v. Löhneysen, A. Rosch, M. Vojta, and P. Wölfle, Rev. Mod. Phys. **79**, 1015 (2007).
[3] P. Gegenwart, Q. Si, and F. Steglich, Nat. Phys. **4**, 286 (2008).
[4] Q. Si and F. Steglich, Science **329**, 1161 (2010).
[5] Y. Zhong, Y.-F. Wang, Y.-Q. Wang, and H.-G. Luo, Phys. Rev. B **87**, 035128 (2013).
[6] Y.-F. Yang, Z. Fisk, H.-O. Lee, J. D. Thompson, and D. Pines, Nature (London) **454**, 611 (2008).
[7] M. Klein, A. Nuber, H. Schwab, C. Albers, N. Tobita, M. Higashiguchi, J. Jiang, S. Fukuda, K. Tanaka, K. Shimada *et al.*, Phys. Rev. Lett. **106**, 186407 (2011).
[8] A. Hewson, *The Kondo Problem to Heavy Fermions* (Cambridge University Press, Cambridge, UK, 1993).
[9] A. Janghorban, M. Lomello-Tafin, J. M. Moreau, and P. Galez, Intermetallics **18**, 2208 (2010).
[10] A. B. Andrews, J. J. Joyce, A. J. Arko, J. D. Thompson, J. Tang, J. M. Lawrence, and J. C. Hemminger, Phys. Rev. B **51**, 3277 (1995).
[11] M. Garnier, K. Breuer, D. Purdie, M. Hengsberger, Y. Baer, and B. Delley, Phys. Rev. Lett. **78**, 4127 (1997).
[12] T. Pillo, J. Hayoz, P. Aebi, and L. Schlapbach, Physica B: Condensed Matter **259**, 1118 (1999).
[13] H. Schwab, M. Mulazzi, J. Jiang, H. Hayashi, T. Habuchi, D. Hirayama, H. Iwasawa, K. Shimada, and F. Reinert, Phys. Rev. B **85**, 125130 (2012).
[14] J. Larrea J., M. B. Fontes, A. D. Alvarenga, E. M. Baggio-Saitovitch, T. Burghardt, A. Eichler, and M. A. Continentino, Phys. Rev. B **72**, 035129 (2005).
[15] A. Schröder, R. van den Berg, and H. v. Löhneysen, Solid State Commun. **65**, 99 (1988).
[16] J. Tang, J. M. Lawrence, and J. C. Hemminger, Phys. Rev. B **48**, 15342 (1993).
[17] C. J. Baddeley, A. W. Stephenson, C. Hardacre, M. Tikhov, and R. M. Lambert, Phys. Rev. B **56**, 12589 (1997).
[18] M. Garnier, D. Purdie, K. Breuer, M. Hengsberger, and Y. Baer, Phys. Rev. B **58**, 9697 (1998).
[19] J. M. Essen, C. Becker, and K. Wandelt, e-J. Surf. Sci. Nanotechnol. **7**, 421 (2009).
[20] The term "superstructure" denotes "some additional (periodic) structure that is superimposed on a given crystalline structure" (Wikipedia), without giving any information on its particular type or origin. We have used this term in our paper wherever we want to describe the bare observation of periodic features with a periodicity larger than the atomic lattice. In contrast, the term "moiré pattern" used further down implies an interpretation as is typically used to describe the superposition effects of two lattices.
[21] K. Heinz, Rep. Prog. Phys. **58**, 637 (1995).
[22] G. Held, S. Uremovic, C. Stellwag, and D. Menzel, Rev. Sci. Instrum. **67**, 378 (1996).
[23] G. Sauerbrey, Z. Phys. **155**, 206 (1959).
[24] R. Pascal, C. Zarnitz, M. Bode, and R. Wiesendanger, Phys. Rev. B **56**, 3636 (1997).
[25] R. Pascal, C. Zarnitz, H. Tödter, M. Bode, M. Getzlaff, and R. Wiesendanger, Appl. Phys. A **66**, 1121 (1998).
[26] J. W. Arblaster, Platinum Met. Rev. **41**, 12 (1997).
[27] M. Ormaza, L. Fernández, S. Lafuente, M. Corso, F. Schiller, B. Xu, M. Diakhate, M. J. Verstraete, and J. E. Ortega, Phys. Rev. B **88**, 125405 (2013).
[28] H. Bethge, D. Heuer, C. Jensen, K. Reshöft, and U. Köhler, Surf. Sci. **331**, 878 (1995).
[29] M. Bode, R. Pascal, M. Dreyer, and R. Wiesendanger, Phys. Rev. B **54**, R8385 (1996).